2026 IEEE/SICE International Symposium on System Integration (SII)
January 11-14, 2026. Cancún, México

Generation of Target Gait Using Biomechanical Relational Network Based on Generative Adversarial Network (BMR-NetGAN)

Ryoya Oba, Yusuke Osawa, Kazunori Kaede and Keiichi Watanuki

Abstract— **Several methods have been developed to capture motion during real-time walking and provide feedback; however, these approaches may not always be suitable for every trainee owing to individual physical differences. In our previous study, we proposed a generative adversarial network (GAN)-based method to generate target gaits for active seniors. The generator incorporated the biomechanical relational network (BMR-Net) to extract inter-variable features of gait. However, the effectiveness of this block in generating individualized target gaits has not yet been verified. In this study, we examined whether the generator incorporating the BMR-Net (BMR-NetGAN) is effective in generating target gaits that reflect individual motion characteristics. In particular, we constructed a 2D transposed convolution GAN, which is generally effective for bidirectional feature extraction in the temporal and variable domains, and a generator without BMR-Net, and compared their results with those of BMR-NetGAN. The results demonstrated that BMR-NetGAN is an effective model for generating ideal gaits that reflect individual motion characteristics, as evidenced by adjustment patterns of lower-limb joint angles on the ZX plane that were not observed in the 2D transposed convolution GAN. Furthermore, an analysis of lower-limb joint motion indicated that BMR-NetGAN may successfully generate target gaits that account for left–right balance in individual participants.**

I. Introduction

The decline in gait ability associated with aging is a major factor influencing the need for nursing care among adults aged 65 years and older in Japan. Therefore, gait support from the stage of "active seniors," who are physically and mentally healthy and motivated to engage in hobbies and work, is highly important. At present, gait support for older adults in nursing care settings is provided mainly through rehabilitation by physical therapists. In recent years, gait feedback training systems have been proposed to address these issues by presenting target values based on the gait patterns of trainees [1]. However, setting target values that consider the physical differences of individual trainees remains a challenge [2], [3]. In particular, the decline in gait ability among active seniors is often caused by factors such as reduced muscle strength and limited joint mobility. In addition, individual differences exist in terms of the gait components that require correction and the magnitude of adjustment needed [4]. Therefore, it is necessary to present individualized target gaits derived from ideal gait features observed in healthy adults, such as joint adjustment and propulsive ground reaction forces, to establish appropriate target values for each active senior.

R. Oba, Y. Osawa, K. Kaede and K. Watanuki are with Graduate School of Science and Engineering, Saitama University, Saitama 338-8570, JAPAN (e-mail: r.oba.056@ms.saitama-u.ac.jp).

In our previous research, we proposed a method for generating target gaits using a machine learning technique known as the generative adversarial network (GAN) to address this issue [5]. A GAN is a data generation framework comprising two networks: a generator and a discriminator. In that study, we constructed a generator based on the transposed convolutional neural network (CNN) employed in the deep convolutional GAN (DCGAN) [6] and a discriminator using a multi-channel deep convolutional neural network (MC-DCNN) combined with a squeeze-and-excitation network (SENet) [7]. In addition, we optimized the training process by introducing identity and cycle consistency losses from the cycle-consistent GAN (CycleGAN) [8], which enables feature transformation between non-ideal and ideal gait features. This enabled the model to learn ideal gait features suitable for trainees while grounding them on the input gait data. Furthermore, in the generator of the proposed method, we developed the biomechanical relational network (BMR-Net) to capture the dependencies and coordination among gait variables across walking phases (Fig. 1).

While diffusion models have recently emerged as a prominent generation technique, they present certain limitations for our specific application. The iterative inference process of diffusion models incurs substantial computational cost [9], making them unsuitable for the real-time feedback required by our proposed gait feedback training system.

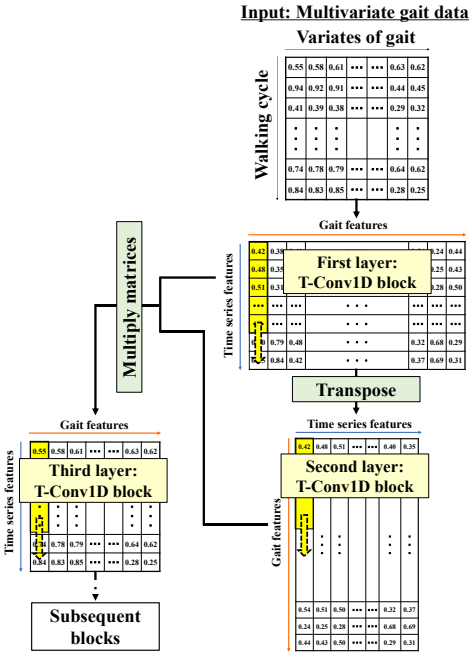

Figure 1. Structure of the BMR-Net (the T-Conv1D block comprises a transposed 1D convolution, layer normalization, and a tanh activation function).

Furthermore, their reliance on large-scale, diverse datasets is problematic [10], given the practical difficulties in collecting comprehensive gait data. In contrast, the core characteristics of our approach, combining CycleGAN and BMR-Net, is its ability to be optimized with a relatively small dataset. In addition, the model efficiently generates high-quality target gaits by preserving the individual characteristics of the input data, applying targeted transformations, and reflecting the dependencies between gait variables.

BMR-Net was embedded in the input layers of the generator. In the first layer, a one-dimensional (1D) transposed convolution was applied in the temporal direction to extract sequential features of each gait variable. In the second layer, the extracted temporal features were transposed and convolved in the variable direction to obtain inter-variable features representing relationships among gait components at each gait phase. In the third layer, the matrix product between the temporal and inter-variable feature vectors was computed to explicitly capture the coordination between the temporal characteristics and inter-variable relationships of each input gait. Through this structure, BMR-Net is expected to represent inter-variable coordination across walking phases. However, whether the introduction of this block is necessary for generating ideal target gaits that reflect the motion characteristics of individual trainees has not yet been examined.

Therefore, this study aimed to examine whether a gait generation model incorporating BMR-Net (referred to as BMR-NetGAN) effectively generates target gaits that account for individual physical differences, with the ultimate aim of developing a gait feedback training system for active seniors. As many falls in older adults are caused by stumbling while walking [11], this study focused on stumbling as the primary target of gait training. First, we constructed a generator based on a two-dimensional transposed CNN (2D-ConvGAN), which is generally considered effective for extracting both temporal and inter-variable features. We compared it with BMR-NetGAN to evaluate whether BMR-NetGAN appropriately reflects inter-variable coordination in target gait generation. Next, BMR-NetGAN was compared with a generator based on a 1D transposed convolution without BMR-Net (1D-ConvGAN) to verify whether the BMR-Net block effectively generates target gaits suitable for active seniors. In all comparisons, the discriminator employed the same structure as that in our previous research, ensuring that the differences in the generated results were solely attributable to the structural differences in the generators directly responsible for gait generation.

II. Generation of Labeled Multivariate Gait Data Related to Stumbling

Input data are required when generating target multivariate gait data using a GAN. In this study, we utilized a previously generated dataset of gaits related to stumbling. The dataset comprised 10,480 multivariate gait data points divided by the stride of the right leg as input data. The experiment was performed on 10 older adult males (mean age 70.6 ± 2.5 years) and eight older adult females (mean age 70.6 ± 2.8 years), all aged 65 years or older and able to walk independently for more than 30 min, as well as eight young adult males (mean age 22.1 ± 0.8 years) and seven young adult females (mean age 20.7 ± 0.5 years). Three experimental conditions were set to avoid the influence of differences in walking speed on gait features. These conditions were subjectively slow speed, subjectively comfortable speed, and subjectively fast speed. In each condition, the belt speed of the treadmill was automatically controlled to keep the participant at the center of the treadmill, allowing the participant to walk at a comfortable speed. The multivariate gait data consisted of the normalized joint angles (those of the trunk, right and left hip, knee, and ankle joints) on the YZ and XZ planes in global coordinates and three components of the normalized ground reaction forces (X, Y, and Z for the right and left legs) as gait variables, as shown in Fig. 2. The sampling frequencies were 250 Hz.

Each multivariate gait datum was assigned to the "gait rarely associated with stumbling" or "gait frequently associated with stumbling" class, which contained 8028 and 2452 data points, respectively. The labeling was performed based on the clustering results obtained using the nearest neighbor method, combined with the dynamic time warping and the elbow method for the right-thumb-to-ground distance (R-TGD), corresponding to each multivariate gait datum, regardless of the experimental conditions. Studies have reported that, as one of the major causes of stumbling in older adults, accidental falls often occur during walking cycles in which the R-TGD becomes markedly small [12]. Consequently, the number of clusters was determined at the point where the within-cluster sum of squared errors converged, resulting in two clusters. All R-TGD values classified into each cluster are shown in Fig. 3. Based on this finding, the clustering results were used for labeling: multivariate gait data included in the cluster with a very large R-TGD during the terminal swing phase (87–100%) were defined as "gait rarely associated with stumbling," whereas multivariate gait data included in the cluster with a tendency toward a small R-TGD during the terminal swing phase were defined as "gait frequently associated with stumbling."

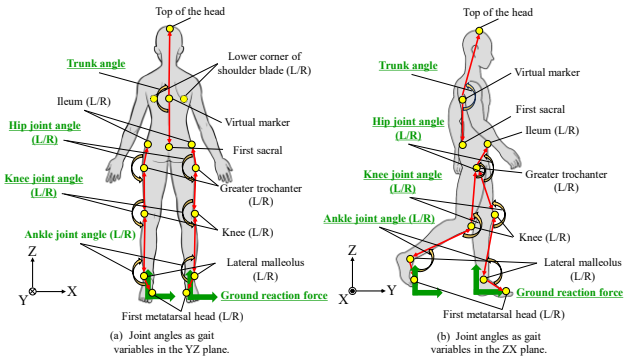

Figure 2. Definitions of gait variables for multivariate gait data.

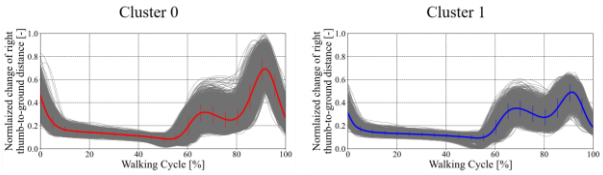

Figure 3. All the thumb-to-ground distances classified into each other (gray),with the mean and standard deviation of Cluster 0 shown in red (8028 data points) and those of Cluster 1 shown in blue (2452 data points).

III. GAIT DATA GENERATION USING THE GAN

A. Construction of BMR-NetGAN and two comparative generator

The structures of BMR-NetGAN, 2D-T-ConvGAN, and 1D-T-ConvGAN are shown in Fig. 4(a), Fig. 4(b), and Fig. 4(c), respectively. The parameters of each layer in BMR-NetGAN were the same as those used in our previous study. The layer-wise parameters of 2D-T-ConvGAN and 1D-T-ConvGAN are summarized in Table 1. In 2D-T-ConvGAN, the multivariate gait data comprising 400 time steps and 20 gait variables were reshaped into the form (400, 20, 1) and treated as single-channel two-dimensional data, to which two-dimensional transposed convolution was applied. This enabled the simultaneous extraction of temporal features and inter-variable relationships using kernels spanning both the temporal and variable directions. In 1D-T-ConvGAN, one-dimensional transposed convolution was applied along the temporal axis, where kernels moved in the time direction to extract features of each variable. Because one-dimensional convolution assigns weights to all gait variables (input channels), correlations among gait variables can be implicitly captured through learning.

B. Generation results of the target gait in each generator

Columns A1, B1, and C1 in Figures 5 and 6 show comparisons of generated gaits. In all columns, the gray solid line represents the test multivariate gait data classified as "gait frequently associated with stumbling," and the red solid line represents the generated results from BMR-NetGAN. Figure 5 also shows the 2D-T-ConvGAN results (blue solid line), while Figure 6 shows the 1D-T-ConvGAN results (green solid line). Both the input and generated gaits were inverse-normalized using the maximum and minimum values of each gait variable across all data. In BMR-NetGAN, the regions with large deviations between the red and gray lines, and in 2D-T-ConvGAN and 1D-T-ConvGAN, the regions with large deviations between the blue and green lines, indicate the portions where gait adjustments were applied relative to the input gaits. For comparison among the generators, characteristic points such as extrema and the mean of the target gait motions were selected. In the input gait data (gray solid line), the corresponding extrema were marked with purple dots, and purple lines were used to indicate the range used for computing the mean values. Furthermore, columns A2, B2, and C2 in Figures 5 and 6 present scatter plots of the differences (adjustments) between the generated and input gaits at each characteristic point, separated by each generator. Each plot in the scatter plots is shown in the same color as that used for the generated gait corresponding to each generator.

In Fig. 5 and Fig. 6 (A2, B2 and C2), scatter plots of the differences (adjustments) between the generated and input gaits at each characteristic point are shown for each generator. Table 2 lists, for each gait variable of interest, the gait-cycle interval and whether the representative value is the local extremum (maximum or minimum) or the mean. Because the trunk angle on the YZ and ZX planes and the hip, knee, and ankle joint angles on the ZX plane do not necessarily exhibit clear extrema within the specified phases, those variables are characterized by the mean within the phase interval. By examining the differences between the generated and input gait variables at these specified phases, we can quantify the degree of adjustment in each joint angle and in the ground-reaction forces, thereby facilitating objective evaluation of the generated results. To support these visual observations with quantitative evidence, we analyzed the adjustment amount (Δ), calculated by subtracting the input gait variable (x) from the generated (y_{gen}). For concise comparison, we use the abbreviations [BMR], [2D], and [1D] for BMR-NetGAN, 2D-T-ConvGAN, and 1D-T-ConvGAN, respectively, within the parenthetical results. We then calculated three metrics for each model: (1) the median adjustment ($\tilde{\Delta}$) to identify overall bias, (2) the interquartile range (IQR(Δ)) to measure adjustment variability, and (3) the slope (a) of a linear regression of Δ against x to determine input-dependency, all reported to three significant figures.

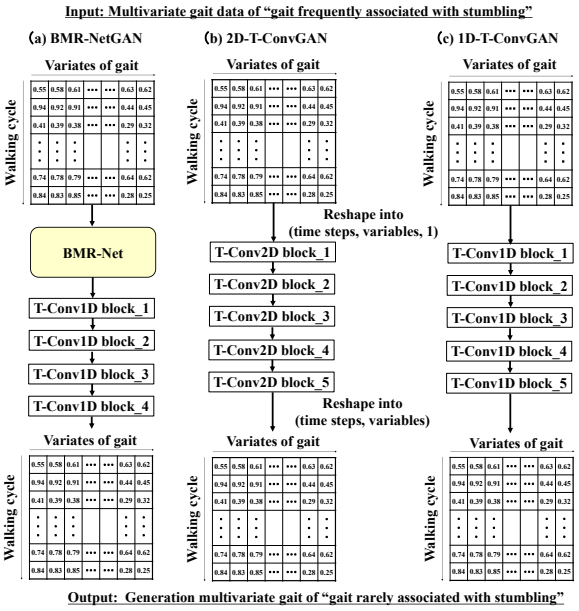

Figure 4. Structure of each generator (the T-Conv1D and T-Conv2D blocks comprise a transposed 1D or 2D convolution in the first layer, followed by layer normalization and a tanh activation function; BMR-Net is shown in Fig. 1).

TABLE I. LAYER DESCRIPTION OF THE 2D-T-CONVGAN AND 1D-T-CONVGAN.

2D-T-ConvGAN	
Layer name	**Layer description**
Input	400 time steps × 20 variables
Reshape	Reshape into (400, 20, 1)
Transposed Conv2d n_1	Filters: 256, kernel size: (7, 5), stride: (1, 1), padding: same
Layer Normalization	-
Activation	Activation function: tanh
Transposed Conv2d n_2	Filters: 128, kernel size: (9, 5), stride: (1, 1), padding: same
Layer Normalization	-
Activation	Activation function: tanh
Transposed Conv2d n_3	Filters: 64, kernel size: (9, 5), stride: (1, 1), padding: same
Layer Normalization	-
Activation	Activation function: tanh
Transposed Conv2d n_4	Filters: 32, kernel size: (9, 5), stride: (1, 1), padding: same
Layer Normalization	-
Activation	Activation function: tanh
Transposed Conv2d n_5	Filters: 20, kernel size: (11, 5), stride: (1, 1), padding: same
Activation	Activation function: tanh
Reshape	Reshape into (400, 20)
Output	400 time steps × 20 variables

1D-T-ConvGAN	
Layer name	**Layer description**
Input	400 time steps × 20 variables
Transposed Conv1d n_1	Filters: 256, kernel size: 7, stride: 1, padding: same
Layer Normalization	-
Activation	Activation function: tanh
Transposed Conv1d n_2	Filters: 128, kernel size: 9, stride: 1, padding: same
Layer Normalization	-
Activation	Activation function: tanh
Transposed Conv1d n_3	Filters: 64, kernel size: 9, stride: 1, padding: same
Layer Normalization	-
Activation	Activation function: tanh
Transposed Conv1d n_4	Filters: 32, kernel size: 9, stride: 1, padding: same
Layer Normalization	-
Activation	Activation function: tanh
Transposed Conv1d n_5	Filters: 20, kernel size: 11, stride: 1, padding: same
Activation	Activation function: tanh
Output	400 time steps × 20 variables

When comparing the multivariate gait data generated by BMR-NetGAN with those generated by 2D-T-ConvGAN, the gaits generated by 2D-T-ConvGAN showed a tendency toward large adjustment magnitudes for the mean values of the knee joint angle on the YZ plane (Fig. 6: [B2]-[2]) ([BMR]: a = -0.381, $\tilde{\Delta}$ = -2.48, IQR(Δ) = 5.33 vs. [2D]: a = -0.451, $\tilde{\Delta}$ = -8.34, IQR(Δ) = 6.16). In addition, the ankle joint angle on the YZ plane of the right leg was adjusted with little variation across different input values (Fig. 6: [B2]-[8]) ([BMR]: a = -0.534, $\tilde{\Delta}$ = -1.94, IQR(Δ) = 2.38 vs. [2D]: a = -0.0923, $\tilde{\Delta}$ = -3.07, IQR(Δ) = 1.08). By contrast, the corresponding adjustments of the knee joint angle on the ZX plane of the right leg during pre-swing to mid-swing (50–87%) (Fig. 6: [B2]-[3]) ([BMR]: a = -0.694, $\tilde{\Delta}$ = 1.13, IQR(Δ) = 7.07 vs. [2D]: a = 0.118, $\tilde{\Delta}$ = -1.05, IQR(Δ) = 2.11), the left knee joint angle on the ZX plane (Fig. 6: [B2]-[6]) ([BMR]: a = -0.811, $\tilde{\Delta}$ = -0.768, IQR(Δ) = 7.48 vs. [2D]: a = -0.0348, $\tilde{\Delta}$ = 1.51, IQR(Δ) = 1.11), and the left hip joint angle on the ZX plane (Fig. 6: [A2]-[10]) ([BMR]: a = -0.623, $\tilde{\Delta}$ = -0.401, IQR(Δ) = 3.11 vs. [2D]: a = 0.195, $\tilde{\Delta}$ = -0.0588, IQR(Δ) = 1.61) generated by 2D-T-ConvGAN showed almost no adjustment, regardless of the input values.

When comparing the multivariate gait data generated by BMR-NetGAN with those generated by 1D-T-ConvGAN, the gaits produced by BMR-NetGAN showed an increase in the hip joint angle on the YZ plane of the right leg during terminal stance to initial swing (31%–62%) (Fig. 7: [A2]-[3]) ([BMR]: a = -0.423, $\tilde{\Delta}$ = 1.18, IQR(Δ) = 2.35 vs. [1D]: a = -0.292, $\tilde{\Delta}$ = -0.628, IQR(Δ) = 1.86). The hip joint angle on the ZX plane of the right leg during initial contact to terminal stance (0%–51%) decreased (Fig. 7: [A2]-[5]) ([BMR]: a = -0.465, $\tilde{\Delta}$ = -1.66, IQR(Δ) = 3.24 vs. [1D]: a = -0.119, $\tilde{\Delta}$ = -0.432, IQR(Δ) = 1.21), whereas that of the left leg increased (Fig. 7: [A2]-[9]) ([BMR]: a = -0.334, $\tilde{\Delta}$ = 1.71, IQR(Δ) = 3.53 vs. [1D]: a = -0.274, $\tilde{\Delta}$ = 0.516, IQR(Δ) = 1.20). In addition, the extrema of the Y component of the ground reaction forces decreased for both the right leg (Fig. 7: [C2]-[4]) ([BMR]: a = -0.444, $\tilde{\Delta}$ = -7.42, IQR(Δ) = 0.739 vs. [1D]: a = -0.0564, $\tilde{\Delta}$ = -0.396, IQR(Δ) = 0.271) and the left leg (Fig. 7: [C2]-[7]) ([BMR]: a = -0.0774, $\tilde{\Delta}$ = -0.522, IQR(Δ) = -0.550 vs. [1D]: a = -0.0652, $\tilde{\Delta}$ = -0.500, IQR(Δ) = 0.195) during terminal stance (31%–51% for the right, 81%–100% for the left). For the mean values of the knee joint angles on the ZX plane during pre-swing to mid-swing (50%–87% for the right, 0%–37% for the left), the gaits generated by 1D-T-ConvGAN showed adjustments in which the right knee joint angle was negative (Fig. 6: [B2]-[3]) ([1D]: a = -0.186, $\tilde{\Delta}$ = -4.04, IQR(Δ) = 2.03) and the left knee joint angle was positive (Fig. 6: [B2]-[6]) ([1D]: a = -0.137, $\tilde{\Delta}$ = 2.68, IQR(Δ) = 1.72). In contrast, the adjustments produced by BMR-NetGAN showed a wider distribution and varied depending on the characteristic points, with adjustments for the right knee (Fig. 6: [B2]-[3]) ([BMR]: a = -0.694, $\tilde{\Delta}$ = 1.13, IQR(Δ) = 7.07) an the left knee (Fig. 6: [B2]-[6]) ([BMR]: a = -0.811, $\tilde{\Delta}$ = -7.68, IQR(Δ) = 7.48).

IV. Discussion

A. Comparison between BMR-NetGAN and 2D-Tconv-GAN

The gaits generated by 2D-T-ConvGAN showed large reductions in the knee joint angle on the YZ plane and the ankle joint angle on the YZ plane during the terminal swing hase. These results suggest that the gaits generated by 2D-T-ConvGAN performed adjustments that promoted flexion–extension motion of the lower-limb joints in the forward direction by strongly pushing off the ground. However, in 2D-T-ConvGAN, the mean values of the joint angles on the ZX plane of each lower-limb joint showed little adjustment regardless of the input values, and no compensatory motions based on hip abduction or external rotation were observed.

TABLE II. WALKING CYCLE AND REPRESENTATIVE VALUES FOR EACH GAIT VARIABLE.

Gait variable	Walking cycle [%]	Representative value
Trunk angle on the YZ plane [°]	0-100	mean
Trunk angle on the XZ plane [°]	0-100	mean
Hip joint angle on the YZ plane of the right leg [°]	31-62	maximum
Hip joint angle on the YZ plane of the right leg [°]	75-100	minimum
Hip joint angle on the ZX plane of the right leg [°]	0-50	mean
Hip joint angle on the ZX plane of the right leg [°]	50-75	mean
Hip joint angle on the YZ plane of the left leg [°]	81-100 and 0-12	maximum
Hip joint angle on the YZ plane of the left leg [°]	25-50	minimum
Hip joint angle on the ZX plane of the left leg [°]	50-100	mean
Hip joint angle on the ZX plane of the left leg [°]	0-25	mean
Knee joint angle on the YZ plane of the right leg [°]	62-75	maximum
Knee joint angle on the YZ plane of the right leg [°]	80-100	minimum
Knee joint angle on the ZX plane of the right leg [°]	50-75	mean
Knee joint angle on the YZ plane of the left leg [°]	12-25	maximum
Knee joint angle on the YZ plane of the left leg [°]	37-50	minimum
Knee joint angle on the ZX plane of the left leg [°]	0-25	mean
Ankle joint angle on the YZ plane of the right leg [°]	50-75	maximum
Ankle joint angle on the YZ plane of the right leg [°]	87-100	minimum
Ankle joint angle on the ZX plane of the right leg [°]	87-100	mean
Ankle joint angle on the YZ plane of the left leg [°]	0-25	maximum
Ankle joint angle on the YZ plane of the left leg [°]	37-50	minimum
Ankle joint angle on the ZX plane of the left leg [°]	37-50	mean
Ground reaction force X component of the right leg [N/kg]	31-50	maximum
Ground reaction force Y component of the right leg [N/kg]	31-50	minimum
Ground reaction force Z component of the right leg [N/kg]	31-50	maximum
Ground reaction force X component of the left leg [N/kg]	81-100	minimum
Ground reaction force Y component of the left leg [N/kg]	81-100	minimum
Ground reaction force Z component of the left leg [N/kg]	81-100	maximum

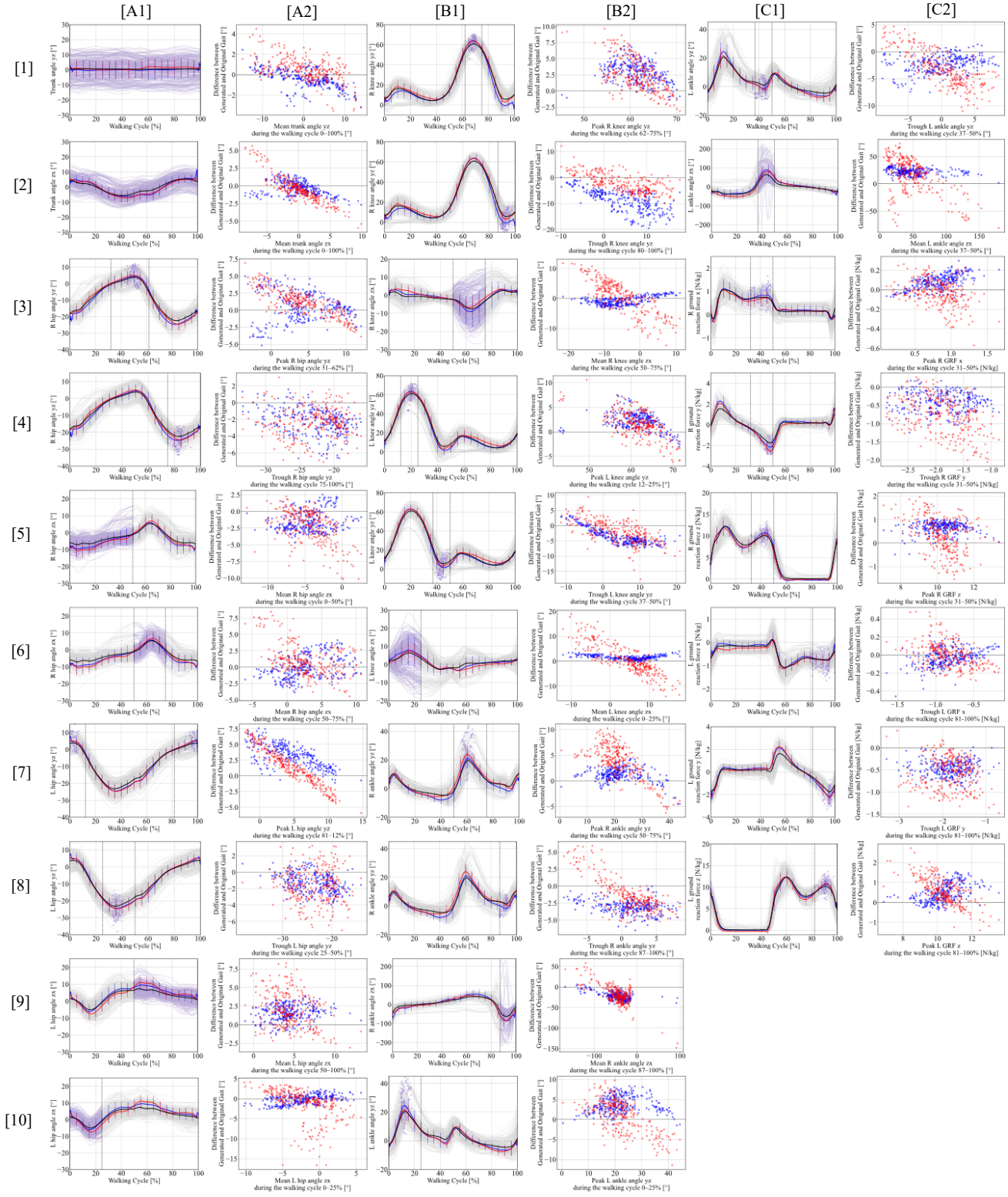

Figure 5. The figures in columns A1, B1, and C1: test multivariate gait data classified as “gait frequently associated with stumbling” (light gray); extrema and mean of the target gait motions (purple dots, purple waveforms); mean and standard deviation of gaits generated by BMR-NetGAN (red); and mean and standard deviation of gaits generated by 2D-T-ConvGAN (blue). The X-axis represents the walking cycle (%), and the Y-axis represents each preprocessed gait variable. Scatter plots in columns A2, B2, and C1: adjustment magnitudes of each generator at the extrema or mean values of the target gait motions. BMR-NetGAN (red dots), 2D-T-ConvGAN (blue dots). X-axis: extrema or mean values of the target gait motions. Y-axis: adjustment gait variable.

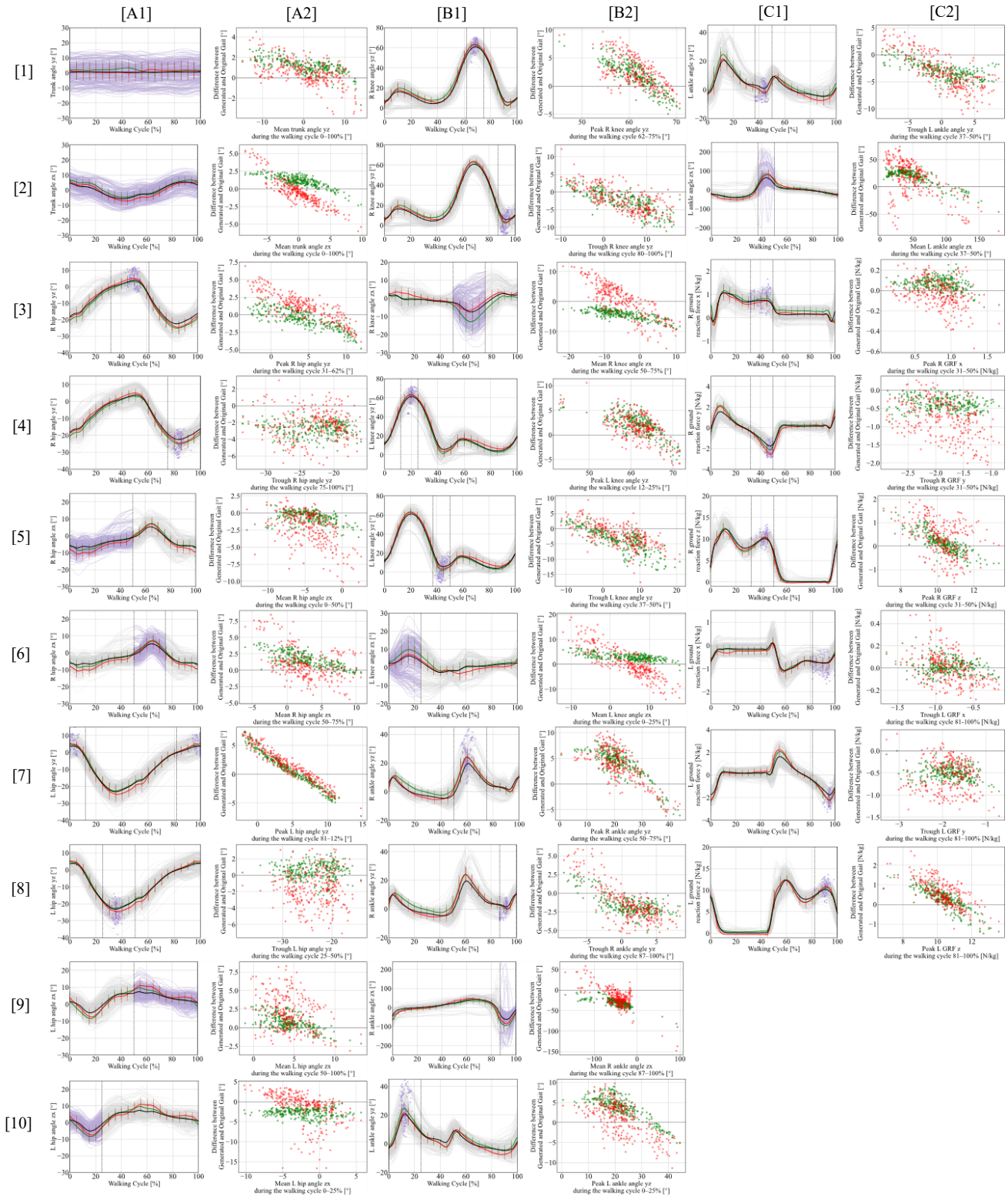

Figure 6. The figures in columns A1, B1, and C1: test multivariate gait data classified as “gait frequently associated with stumbling” (light gray); extrema and mean of the target gait motions (purple dots, purple waveforms); mean and standard deviation of gaits generated by BMR-NetGAN (red); and mean and standard deviation of gaits generated by 1D-T-ConvGAN (blue). The X-axis represents the walking cycle (%), and the Y-axis represents each preprocessed gait variable. Scatter plots in columns A2, B2, and C1: adjustment magnitudes of each generator at the extrema or mean values of the target gait motions. BMR-NetGAN (red dots), 1D-T-ConvGAN (blue dots). X-axis: extrema or mean values of the target gait motions. Y-axis: adjustment gait variable.

These findings indicate that, while 2D-T-ConvGAN strongly learned the ideal gait features necessary to secure greater toe clearance, it did not necessarily generate target values that reflect individual physical differences. This limitation is likely because 2D-T-ConvGAN processes the temporal and variable directions simultaneously through two-dimensional convolution; since it convolves adjacent variables at the same time, it captures only local inter-variable correlations, is sensitive to the ordering of variables, and has difficulty representing long-range dependencies across distant joints. In other words, it can directly capture "stumble-resistant" patterns at a given time but may not sufficiently fails to sufficiently reflect inter-variable relationships that characterize physical individual differences.

By contrast, in the gaits generated by BMR-NetGAN, the joint angles on the ZX plane varied according to the input data, and the adjustment values were widely distributed. Notably, the adjustments of the knee joint angles on the ZX plane revealed that, for some input data, compensatory circumduction of the knee joint induced by external hip rotation was permitted, suggesting that the model generated gaits that allowed compensatory movements. This can be explained by the fact that BMR-NetGAN first extracts temporal features in the initial layer and then captures inter-variable relationships based on these temporal features, which enables it to more efficiently learn inter-variable coordination at each gait phase compared with 2D-T-ConvGAN. Consequently, BMR-NetGAN was able to generate gaits that retained globally shared "stumble-resistant" features while also allowing diverse adjustments and compensatory movements based on individual differences at the local level. Furthermore, unlike 2D-T-ConvGAN, which also employs kernels along the variable axis, BMR-NetGAN captured the ideal gait features using temporal kernels only, thereby likely achieving more efficient learning.

B. Comparison between BMR-NetGAN and 1D-Tconv-GAN

Compared with the gaits generated by 1D-T-ConvGAN, those generated by BMR-NetGAN showed an increase in the right hip joint angle on the YZ plane and a decrease in the left hip joint angle on the YZ plane during terminal stance to initial swing. In addition, they showed a decrease in the Y components of the ground reaction forces of both legs during terminal stance. These results suggest that, at terminal stance, BMR-NetGAN promoted hip extension and generated movements that ensured a forward propulsive force.

Regarding the knee joint angles on the ZX plane, the gaits generated by 1D-T-ConvGAN consistently suppressed lateral knee motion regardless of the input values, whereas those generated by BMR-NetGAN varied depending on the characteristic points. Focusing on the adjustments of the extrema of the right knee joint angle on the YZ plane during mid-swing, the BMR-NetGAN outputs showed different adjustment results for data points with relatively small flexion (50–60°) (Fig. 7). The data with flexion adjustments of less than 5° were grouped as Cluster A, and those with adjustments of 5° or more were grouped as Cluster B. For Cluster A, the extrema of the left knee joint angle on the YZ plane during mid-swing were approximately the same as those of the right knee joint angle in both the original and generated gaits. In addition, the generated results for the mean values of the knee joint angle on the ZX plane during pre-swing to mid-swing permitted hip external rotation. These findings suggest that the gait characteristics of Cluster A were defined by limited bilateral knee flexion ability, and compensatory circumduction through bilateral hip external rotation was allowed to ensure sufficient toe clearance.

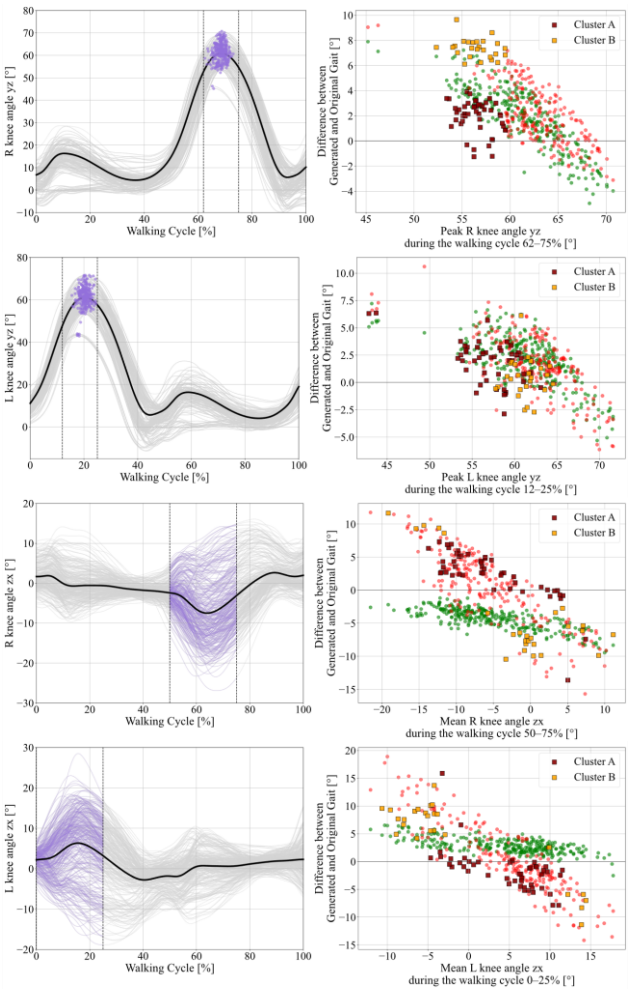

Figure 7. The left figures: test multivariate gait data classified as "gait frequently associated with stumbling" (light gray); extrema and mean of the target gait motions (purple dots, purple waveforms); mean and standard deviation of gaits generated by BMR-NetGAN (red); and mean and standard deviation of gaits generated by 1D-T-ConvGAN (green). The X-axis represents the walking cycle (%), and the Y-axis represents each preprocessed gait variable. The right figures: adjustment magnitudes of each generator at the extrema or mean values of the target gait motions. BMR-NetGAN (red dots), 1D-T-ConvGAN (green dots). Adjustment magnitudes of Cluster A are shown in dark brown (47 data points) and those of Cluster B in yellow (27 data points). Cluster A corresponds to input data with extrema of the right knee joint angle on the YZ plane during mid-swing distributed between 50° and 60°, with adjustment magnitudes of less than 5°. Cluster B corresponds to input data with the same extrema range but adjustment magnitudes of 5° or greater. X-axis: extrema or mean values of the target gait motions. Y-axis: adjustment gait variable.

For Cluster B, the extrema of the knee joint angles on the YZ plane during mid-swing showed that the original flexion was greater than that of the right knee, and the generated results exhibited smaller adjustments in the right knee flexion angle. Moreover, the generated results for the mean values of the bilateral knee joint angles on the ZX plane during pre-swing to mid-swing included adjustments permitting hip external rotation. Among five data points with right knee ZX plane angles between -20° and -10° and left knee ZX plane angles between 10° and 15°, the original gaits represented extreme hip internal rotation.

By contrast, the generated results adjusted the hip joint angles toward external rotation. These findings indicate that Cluster B gaits involved asymmetry in knee joint motion during swing, and BMR-NetGAN adjusted this imbalance to promote forward propulsion of the lower limbs. Overall, these results demonstrate that BMR-NetGAN can generate gaits that account for individual physical characteristics, including the correction of left–right imbalances in lower-limb joint motion. Furthermore, our previous research has shown that this model can generate values that consider both individual differences and the validity of human gait motion. In conclusion, the model can generate a target gait equivalent to the gait adjustments guided by physical therapists in a clinical setting.

V. Conclusion

In this study, we examined whether the gait generation model incorporating BMR-NetGAN effectively generates target gaits that reflect individual physical characteristics, with the aim of developing a gait feedback training system for active seniors. In particular, we constructed a 2D transposed convolutional GAN, which performs bidirectional feature extraction in the temporal and variable directions, and a 1D transposed convolutional GAN without BMR-Net. By comparing their generated results with those of the proposed model, we confirmed that BMR-NetGAN can effectively generate ideal gaits that reflect individual motion characteristics, as exemplified by adjustments in lower-limb joint angles on the ZX plane that were not observed in the 2D transposed convolutional GAN. Furthermore, the adjustment patterns of lower-limb joint movements suggested that BMR-NetGAN can generate target gaits that consider the left–right balance of participants. Taken together, these findings indicate that BMR-NetGAN is useful for generating ideal gaits that reflect the characteristics of individual body movements. Although this study focused primarily on gait generation, the structural characteristics of the proposed model suggest possible applications to broader biomechanical domains, such as support for athletic performance and other forms of movement analysis.

References

[1] K. McMaster, M. H. Cole, D. Chalkley, and M. W. Creaby, "Gait biofeedback training in people with Parkinson's disease: a pilot study," *J. Neuroeng. Rehabil.*, vol. 19, Art. no. 72, 2022.

[2] M. Bonilla-Yanez, S. A. Kettlety, J. M. Finley, N. Schweighofer, and K. A. Leech, "Gait speed and individual characteristics are related to specific gait metrics in neurotypical adults," *Sci. Rep.*, vol. 12, Art. no. 6554, 2022.

[3] B. X. W. Liew, R. Senden, D. Rugamer, E. Sommer, K. Meijer, Q. Mei, R. Foster, and M. Taylor, "Predicting normative walking biomechanics across the lifespan using seven simple features," medRxiv, 2025.

[4] J. Wang, Y. Li, G.-Y. Yang, and K. Jin, "Age-related dysfunction in balance: A comprehensive review of causes, consequences, and interventions," *Aging Dis.*, vol. 16, pp. 714–737, 2024.

[5] R. Oba, Y. Osawa, K. Watanuki, and K. Hori, "Gait data generation using generative adversarial network based on human dynamics," *Trans. JSME*, vol. 91, no. 6, Art. no. 25-00003, 2025.

[6] A. Radford, L. Metz, and S. Chintala, "Unsupervised representation learning with deep convolutional generative adversarial networks," *arXiv preprint* arXiv:1511.06434, 2015.

[7] J. Hu, L. Shen, and G. Sun, "Squeeze-and-excitation networks," in *Proc. IEEE Conf. Comput. Vis. Pattern Recognit. (CVPR)*, 2018, pp. 7132–7141.

[8] J.-Y. Zhu, T. Park, P. Isola, and A. A. Efros, "Unpaired image-to-image translation using cycle-consistent adversarial networks," in *Proc. IEEE Int. Conf. Comput. Vis. (ICCV)*, 2017, pp. 2223–2232.

[9] J. Ho, A. Jain, and P. Abbeel, "Denoising diffusion probabilistic models," in *Proc. Adv. Neural Inf. Process. Syst. (NeurIPS)*, 2020, pp. 6840–6851.

[10] N. Ma, S. Tong, H. Jia, H. Hu, Y.-C. Su, M. Zhang, X. Yang, Y. Li, T. Jaakkola, X. Jia, and S. Xie, "Scaling inference time compute for diffusion models," in *Proc. IEEE/CVF Conf. Comput. Vis. Pattern Recognit. (CVPR)*, 2025.

[11] A. J. Blake, K. Morgan, M. J. Bendall, H. Dallosso, S. B. J. Ebrahim, T. H. D. Arie, P. H. Fentem, and E. J. Bassey, "Falls by elderly people at home: Prevalence and associated factors," *Age Ageing*, vol. 17, pp. 365–372, 1988.

[12] M. P. Mills, R. S. Barrett, and S. Morrison, "Toe clearance variability during walking in young and elderly men," *Gait Posture*, vol. 28, no. 1, pp. 101–107, 2008.